

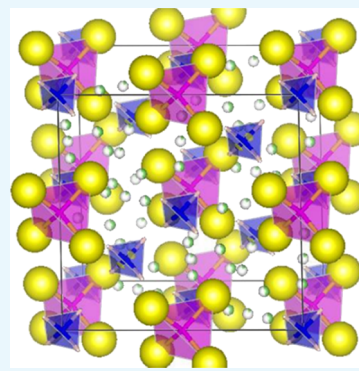
Mechanochemically Prepared Li₂S–P₂S₅–LiBH₄ Solid Electrolytes with an Argyrodite Structure

Atsushi Sakuda,[†] Akihiro Yamauchi,[†] So Yubuchi,[†] Naoto Kitamura,[‡] Yasushi Idemoto,[‡] Akitoshi Hayashi,^{*,†} and Masahiro Tatsumisago[†]

[†]Department of Applied Chemistry, Graduate School of Engineering, Osaka Prefecture University, 1-1 Gakuen-cho, Naka-ku, Osaka 599-8531, Japan

[‡]Department of Pure and Applied Chemistry, Faculty of Science and Technology, Tokyo University of Science, 2641 Yamazaki, Noda, Chiba 278-8510, Japan

ABSTRACT: Solid electrolytes with compositions of $(100 - x)(0.75\text{Li}_2\text{S}\cdot0.25\text{P}_2\text{S}_5)\cdot x\text{LiBH}_4$ (mol %, $0 \leq x \leq 100$) were mechanochemically prepared from the $75\text{Li}_2\text{S}\cdot25\text{P}_2\text{S}_5$ (mol %) glass and LiBH₄ crystal. The samples with $x \geq 43$ have crystalline phases and those with $x \leq 33$ formed a glassy phase. The crystalline phase was identified as argyrodite $\text{Li}_6\text{PS}_5(\text{BH}_4)$. The $x = 50$ sample formed a crystalline phase and demonstrated a high lithium-ion conductivity of $1.8 \times 10^{-3} \text{ S cm}^{-1}$ at 25°C with an activation energy of 16 kJ mol^{-1} . The argyrodite-type crystal with a BH₄⁻ anion that occupies the halide site is a novel and promising solid electrolyte.



1. INTRODUCTION

All-solid-state lithium-ion batteries have attracted significant attention as next-generation batteries.¹ The performance of the all-solid-state batteries strongly depends on the conductivities of the solid electrolytes.² Recently, sulfide-based solid electrolytes have become more widespread because they possess high conductivities ($>10^{-3} \text{ S cm}^{-1}$ at 25°C)^{2–8} and good mechanical properties for the formation of effective interfaces between solids.^{9,10} Adding lithium halides to glass electrolytes is well-known to be effective in improving conductivity. For example, LiI in addition to sulfide-based glasses resulted in a high conductivity of $10^{-3} \text{ S cm}^{-1}$ at 25°C .^{3,11,12} Argyrodite Li₆PS₅X (X = Cl, Br, and I) also displayed high conductivities of over $10^{-3} \text{ S cm}^{-1}$ at 25°C .^{13–16}

Lithium borohydride (LiBH₄) has been reported to exhibit high lithium-ion conductivity and high stability to reduction at high temperatures.^{17,18} LiBH₄ is also attractive as an additive salt in the solid electrolyte. Previous investigations^{19–21} have revealed that the addition of LiBH₄ to sulfide-based glassy solid electrolytes by a mechanochemical process increases their conductivities.²⁰ The glasses were fabricated with compositions ranging from $x = 0$ to 33 in $(100 - x)(0.75\text{Li}_2\text{S}\cdot0.25\text{P}_2\text{S}_5)\cdot x\text{LiBH}_4$ (mol %). It was discovered that crystals precipitated in samples with $x \geq 43$.^{19,20} A similar crystalline phase was also observed in the LiBH₄–P₂S₅ system.²¹

In this study, we mechanochemically prepared solid electrolytes with crystalline phases with a composition of $(100 - x)(0.75\text{Li}_2\text{S}\cdot0.25\text{P}_2\text{S}_5)\cdot x\text{LiBH}_4$. We determined that the prepared crystal had an argyrodite phase and that the BH₄⁻ anion occupied the halide site of the argyrodite structure. The solid

electrolytes with the argyrodite-type phase exhibited a high lithium-ion conductivity of $1.8 \times 10^{-3} \text{ S cm}^{-1}$ at 25°C .

2. METHODS

Solid electrolytes with compositions of $(100 - x)(0.75\text{Li}_2\text{S}\cdot0.25\text{P}_2\text{S}_5)\cdot x\text{LiBH}_4$ (mol %, $43 \leq x \leq 100$) were prepared via a mechanochemical process. In addition, $(100 - x)(0.75\text{Li}_2\text{S}\cdot0.25\text{P}_2\text{S}_5)\cdot x\text{LiBH}_4$ (mol %, $x = 0$ and 33) glasses were prepared by the same process for comparison. Li₂S (Idemitsu Kosan, 99.9%), P₂S₅ (Aldrich, 99%), and LiBH₄ (Aldrich, 90%) were used as starting materials. First, a stoichiometrically calculated mixture of Li₂S and P₂S was mechanically milled in a 225 mL ZrO₂ pot with 2500 ZrO₂ balls (4 mm in diameter) using a planetary ball mill (Fritsch, Pulverisette 5) at 213 rpm for 45 h. The resulting $75\text{Li}_2\text{S}\cdot25\text{P}_2\text{S}_5$ glass was then mixed with a calculated amount of LiBH₄ crystals. Mechanical milling of this mixture was performed in a 45 mL ZrO₂ pot with 500 ZrO₂ balls (4 mm in diameter) using a planetary ball mill (Fritsch, Pulverisette 7) at 510 rpm for 15 h to form the $(100 - x)(0.75\text{Li}_2\text{S}\cdot0.25\text{P}_2\text{S}_5)\cdot x\text{LiBH}_4$ solid electrolytes. All processes were performed under a dry Ar atmosphere. The compositions of the $(100 - x)(0.75\text{Li}_2\text{S}\cdot0.25\text{P}_2\text{S}_5)\cdot x\text{LiBH}_4$ samples are given in Table 1. The ratio of BH₄⁻ and PS₄³⁻ was varied by integral ratios.

Received: March 2, 2018

Accepted: May 7, 2018

Published: May 21, 2018

Table 1. Compositions of $(100 - x)(0.75\text{Li}_2\text{S}\cdot0.25\text{P}_2\text{S}_5)\cdot x\text{LiBH}_4$ Samples

x	composition
0	=Li ₃ PS ₄
33	=50Li ₃ PS ₄ ·50LiBH ₄
43	=40Li ₃ PS ₄ ·60LiBH ₄
50	=33Li ₃ PS ₄ ·67LiBH ₄
54	=30Li ₃ PS ₄ ·70LiBH ₄
82	=10Li ₃ PS ₄ ·90LiBH ₄
100	=LiBH ₄

X-ray diffraction (XRD) measurements with Cu K α radiation ($\lambda = 0.1542$ nm) were performed using a diffractometer (Rigaku, Ultima IV). An air-sealing holder was used to prevent exposure of the samples to air. Rietveld refinements were performed using RIETAN-FP.²² The XRD data were collected in the 2θ range between 10° and 80° at a scan rate of $0.1^\circ \text{ min}^{-1}$ and a step size of 0.02° . The structure was refined starting from the published XRD data by Rayavarapu et al.¹⁵ Differential scanning calorimetry (DSC) was performed on the obtained samples sealed in an Al pan in a glovebox using a thermal analyzer (Seiko Instruments Inc., DSC6200) at a scanning rate of $10^\circ \text{ C min}^{-1}$. Raman spectra were obtained using a Raman spectrometer (HORIBA, LabRAM HR-800) with a 325 nm He–Cd laser. To measure electrical conductivities, the samples were first placed under 360 MPa pressure at room temperature to form pellets 10 mm in diameter and 1–1.5 mm in thickness. ac impedance measurements were performed using an impedance analyzer (Solartron, 1260) in the frequency range of 0.1 Hz to 8 MHz. The all-solid-state cells were constructed in the same way as previously reported elsewhere except that newly developed solid electrolytes were used.⁹

3. RESULTS AND DISCUSSION

Figure 1 shows the XRD patterns of the mechanochemically prepared $(100 - x)(0.75\text{Li}_2\text{S}\cdot0.25\text{P}_2\text{S}_5)\cdot x\text{LiBH}_4$ samples. The XRD patterns for $x = 0$ and 33 display characteristic halo

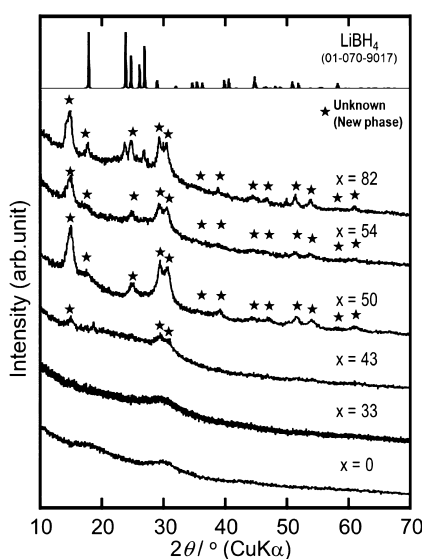


Figure 1. XRD patterns of as-milled $(100 - x)(0.75\text{Li}_2\text{S}\cdot0.25\text{P}_2\text{S}_5)\cdot x\text{LiBH}_4$ (mol %, $0 \leq x \leq 82$) solid electrolytes. The XRD pattern of LiBH₄ from the data of Soulié et al.²³ is shown for comparison.

patterns; it has been previously reported that the samples with $x \leq 33$ have a glassy state.²⁰ For the samples with $43 \leq x \leq 82$, unknown diffraction peaks, which were not attributed to the starting materials of Li₂S, P₂S₅, or LiBH₄, were observed in the XRD patterns. In the XRD pattern of the $x = 82$ sample, the peaks attributed to LiBH₄²³ were also observed, suggesting that unreacted LiBH₄ was present in a small quantity in the $x = 82$ sample.

The DSC curves of the $(100 - x)(0.75\text{Li}_2\text{S}\cdot0.25\text{P}_2\text{S}_5)\cdot x\text{LiBH}_4$ samples and the LiBH₄ crystal are shown in Figure 2.

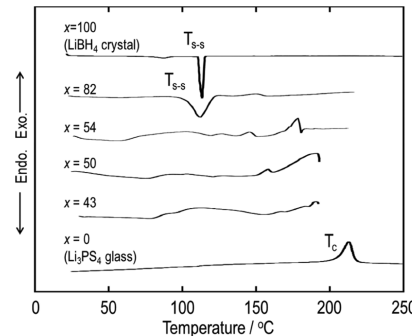


Figure 2. DSC curves of $(100 - x)(0.75\text{Li}_2\text{S}\cdot0.25\text{P}_2\text{S}_5)\cdot x\text{LiBH}_4$ (mol %, $0 \leq x \leq 100$) solid electrolytes and LiBH₄ crystal.

Gas generations were detected in Li₂S–P₂S₅–LiI samples under 220°C . For example, the weight loss due to the gas generation was detected at 180°C in the $x = 50$ sample by thermogravimetric analysis conducted before the DSC measurements. Thus, the DSC measurements were conducted below the gas generation temperature. The gas generation would be caused by thermal decomposition of the samples. This suggests that this series of materials can be prepared only by the low-temperature process. An endothermic peak at 113°C in the LiBH₄ curve can be attributable to a phase transition from orthorhombic to hexagonal,²⁴ which is observed at 113°C . A similar endothermic peak is not observed for the $(100 - x)(0.75\text{Li}_2\text{S}\cdot0.25\text{P}_2\text{S}_5)\cdot x\text{LiBH}_4$ samples except for the $x = 82$ sample, which partially includes the LiBH₄ crystal. The DSC curves for the $x = 43$, 50, and 54 samples exhibit broad exothermic peaks at approximately $60\text{--}160^\circ\text{C}$. The $x = 0$ sample has an exothermic peak at 213°C , which has been reported to arise from the crystallization of the glass.²⁵ Thus, it is considered that the broad exothermic profiles observed in the $x = 43$, 50, and 54 samples are attributable to the crystallization and/or increase in the crystallinity.

Figure 3 shows the Raman spectra of the $(100 - x)(0.75\text{Li}_2\text{S}\cdot0.25\text{P}_2\text{S}_5)\cdot x\text{LiBH}_4$ samples and the LiBH₄ crystal between 200 and 3000 cm^{-1} . The band at 420 cm^{-1} can be attributed to the PS₄³⁻ ions²⁶ and is observed for samples containing LiBH₄. Samples containing LiBH₄ also display a broad band at approximately 2330 cm^{-1} . This band can be attributed to BH₄⁻ ion vibrations. Vibration of the internal BH₄⁻ ions results in strong bands at 2275 and 2300 cm^{-1} for the orthorhombic low-temperature phase and a broad band at approximately 2300 cm^{-1} for the hexagonal high-temperature phase.²⁷ The bands observed in the spectra of the samples with $x \leq 54$ are similar to those observed in the high-temperature phase. The band observed in the spectrum of the samples with $x = 82$ is similar to that observed in the low-temperature phase.²⁷ The rotation of the BH₄⁻ ions probably accelerates in the high-temperature phase,^{28,29} where there is delocalization of

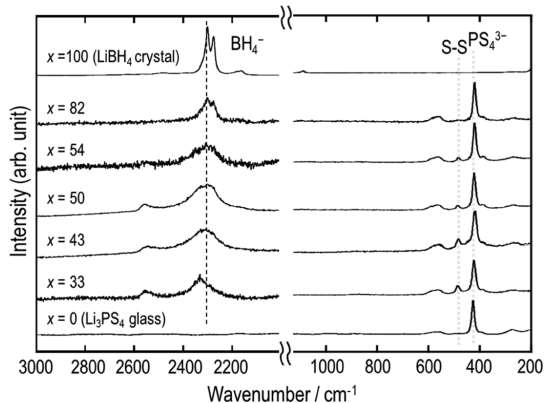


Figure 3. Raman spectra of $(100 - x)(0.75\text{Li}_2\text{S}\cdot0.25\text{P}_2\text{S}_5)\cdot x\text{LiBH}_4$ (mol %, $0 \leq x \leq 100$) solid electrolytes and LiBH_4 crystal.

the negative charge on the BH_4^- ions. The BH_4^- and Li^+ ions have weakened electrostatic interactions in the high-temperature LiBH_4 phase and the $x \leq 54$ samples prepared in this study.

The temperature dependence of the conductivities of the $50(0.75\text{Li}_2\text{S}\cdot0.25\text{P}_2\text{S}_5)\cdot50\text{LiBH}_4$ solid electrolyte ($x = 50$) and $75\text{Li}_2\text{S}\cdot25\text{P}_2\text{S}_5$ glass ($x = 0$) is shown in Figure 4. The LiBH_4

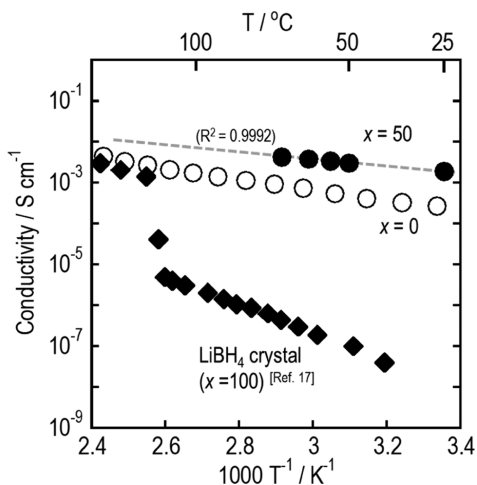


Figure 4. Temperature dependence of the conductivity of as-obtained $50(0.75\text{Li}_2\text{S}\cdot0.25\text{P}_2\text{S}_5)\cdot50\text{LiBH}_4$ ($x = 50$) solid electrolytes, $75\text{Li}_2\text{S}\cdot25\text{P}_2\text{S}_5$ ($x = 0$) glass, and LiBH_4 crystal (from Matsuo et al.,¹⁷ $x = 100$).

crystal data reported by Matsuo et al.¹⁷ are also shown for comparison. In the temperature range from 20 to 70 °C, the conductivities of the samples with $x = 50$ obey the Arrhenius law and the conduction activation energy is determined to be 16 kJ mol⁻¹. Although higher conductivities are obtained above 70 °C, accurate values are difficult to measure because of the extremely low resistance. The crystalline sample with $x = 50$ exhibits a higher conductivity (1.8×10^{-3} S cm⁻¹) at 25 °C than those of the $75\text{Li}_2\text{S}\cdot25\text{P}_2\text{S}_5$ glass samples (2.7×10^{-4} S cm⁻¹) and the LiBH_4 crystal high-temperature phase (1.0×10^{-3} S cm⁻¹ at 115°C¹⁷).

The influence of composition on the conductivity at room temperature and activation energies for the $(100 - x)(0.75\text{Li}_2\text{S}\cdot0.25\text{P}_2\text{S}_5)\cdot x\text{LiBH}_4$ solid electrolytes is shown in Figure 5. The experimental results of the glassy electrolytes with $x = 0, 11$, and 33^{20} are also shown. In the glass-forming region,

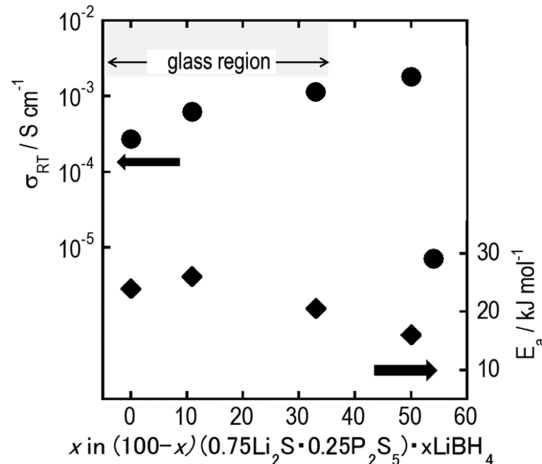


Figure 5. Influence of the composition on conductivities and conduction activation energies of $(100 - x)(0.75\text{Li}_2\text{S}\cdot0.25\text{P}_2\text{S}_5)\cdot x\text{LiBH}_4$ (mol %, $0 \leq x \leq 54$) solid electrolytes.

conductivity of the glasses increases and the activation energies decrease with increasing LiBH_4 content. The $x = 50$ crystalline sample displays higher conductivity and lower activation energy than those of the other compositions, suggesting that the crystalline phase exhibits high lithium-ion conductivity. The conductivity dramatically decreased in the $x = 54$ and $x = 82$ samples. The conductivity of the $x = 82$ sample was less than 10^{-6} S cm⁻¹ at 25 °C. The reason of the decrease of the conductivity has not been clarified yet. One possibility is that the highly resistive amorphous materials as LiBH_4 were formed at grain boundary of the highly conducting argyrodite crystallites in the sample. The possibility of decreasing the conductivities of crystalline phase with argyrodite phase was also not denied at the present stage.

To characterize the crystal structure, samples with higher crystallinity were prepared by heat treatment at 130 °C. Figure 6a shows the XRD patterns of the as-obtained and heat-treated samples with an $x = 50$ composition. The intensities of the diffraction peaks observed in the spectra of the as-obtained sample increase with the heat treatment, indicating that the exothermic peaks observed in Figure 2 can be attributed to crystallization. The DSC results indicate that the $x > 33$

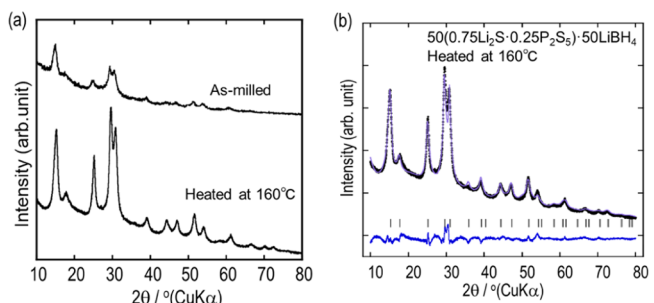


Figure 6. (a) XRD patterns of $50(0.75\text{Li}_2\text{S}\cdot0.25\text{P}_2\text{S}_5)\cdot50\text{LiBH}_4$ (mol %) solid electrolytes before and after heat treatment (top and bottom, respectively). (b) Rietveld refinement pattern of the heated $x = 50$ sample. The solid line represents the calculated intensities, and dotted line represents the observed intensities. Vertical marks below the lines indicate the positions of the allowed Bragg reflections. The curve at the bottom shows the difference between the observed and calculated intensities on the same scale.

Table 2. Refined Structural Parameters of $\text{Li}_6\text{PS}_5(\text{BH}_4)$ in Space Group $F\bar{4}3m$ (Cubic) at Room Temperature^a

atom	site	site occupancy	x	y	z	$10^2 \times B/\text{nm}^2$
Li1	48h	0.44	0.3393(3)	=Li1(x)	0.015(5)	6.95
Li2	24g	0.12	1/4	1/4	0.01(4)	6.95
P1	4b	1	1/2	1/2	1/2	2.7(4)
B1	4a	0.67(4)	0	0	0	2.4(10)
S1	4a	=1 - B1(g)	=B1(x)	=B1(y)	=B1(z)	=B1(B)
B2	4d	=1 - B1(g)	3/4	3/4	3/4	1
S2	4d	=1 - B2(g)	=B2(x)	=B2(y)	=B2(z)	=B2(B)
S3	16e	1	0.3813(6)	=S3(x)	=S3(x)	0.3(3)
H1	16e	=B1(g)	0.07	=H1(x)	=-H1(x)	1
H2	16e	=1 - H1(g)	0.68	=H2(x)	=H2(x)	1

^aLattice parameter: $a = 1.001(8)$ nm. R-factor: $R_{wp} = 3.36\%$, $R_p = 2.61\%$, $R_e = 1.27\%$, and $S = 2.65$.

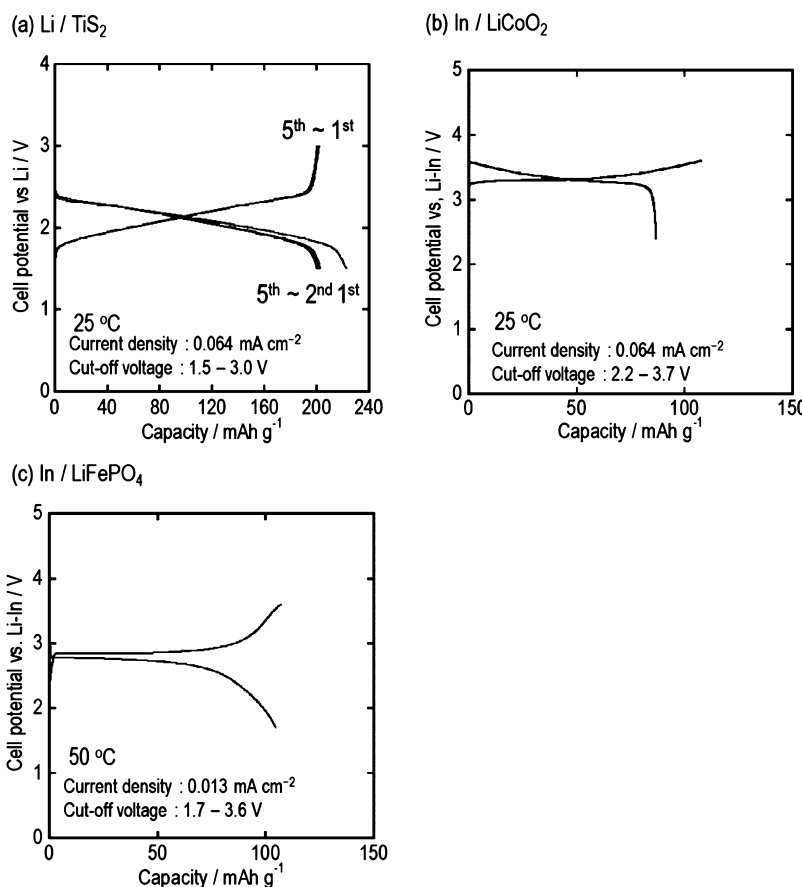


Figure 7. Charge–discharge curves of all-solid-state cells using 50(0.75Li₂S·0.25P₂S₅)·50LiBH₄: (a) Li/TiS₂, (b) In/LiCoO₂, and (c) In/LiFePO₄. The operating conditions are shown in the figures.

samples are primarily composed of crystal and glass components. The pattern of the newly formed crystal phase is similar to that of the argyrodite-type crystal Li₆PS₅X (X = Cl, Br, and I),^{14,15} suggesting that the obtained crystalline phase is argyrodite-type. The ionic radii of Cl⁻ (0.168 nm) and Br⁻ (0.195 nm) ions are similar to that of BH₄⁻ ions (0.205 nm).³⁰ Thus, we presume that the Li_{7-x}PS_{6-x}(BH₄)_x crystal precipitates, where BH₄⁻ ions occupy the sites of Cl⁻ or Br⁻ ions in the Li_{7-x}PS_{6-x}X_x crystal. The structural model of the Li₆PS₅Cl crystal reported by Rayavarapu et al.¹⁵ was used as a starting point for the Rietveld refinement.

Figure 6b shows the Rietveld refinement pattern of the heated $x = 50$ sample. The refined structural parameters for Li₆PS₅(BH₄) obtained from the Rietveld refinements are

summarized in Table 2. Peak indexing of the XRD data suggests that the new phase exhibits argyrodite structure in the space group $F\bar{4}3m$ with a lattice parameter of 1.001(8) nm. The BH₄⁻ and S²⁻ ions are disordered over the 4a site (0 0 0) (67% BH₄, 33% S) and 4d site (3/4 3/4 3/4) (33% BH₄, 67% S). It was previously reported that disorder in the S²⁻/X⁻ (X = Cl, Br, and I) distribution promotes lithium-ion mobility in argyrodite-type crystals.¹⁵ The large I⁻ ions cannot be exchanged for S²⁻ ions, and the resulting Li₆PS₅I is more ordered and exhibits only moderate conductivity. The disorder in the S²⁻/BH₄⁻ distribution indicates that the Li₆PS₅(BH₄) crystal exhibits high lithium-ion conductivity. The increase in the lattice parameter should also affect the conductivity of the crystal. The argyrodite-type Li₆PS₅(BH₄) phase refined here is a

novel lithium-ion conductor. In this study, the Rietveld refinements were performed using the XRD data of the low crystallinity sample. The Rietveld refinements for the neutron diffraction data of high crystallinity samples are necessary to determine more accurate atomic coordinates for hydrogen and lithium.

The conductivity of the heat-treated $x = 50$ sample was 1.9×10^{-3} S cm $^{-1}$ at 25 °C, which is almost similar to that of as-obtained samples. It is clear that the Li₆PS₅(BH₄) phase is more Li-rich compared with the (100 – x)(0.75Li₂S-0.25P₂S₅)· x LiBH₄ ($x = 50$) solid electrolytes. This suggests that the glass matrix of the $x = 50$ sample has a lower Li $^{+}$ ion concentration than its nominal composition. However, the $x = 50$ solid electrolytes that included the Li₆PS₅(BH₄) phase and glass matrix exhibited a high lithium-ion conductivity of more than 10 $^{-3}$ S cm $^{-1}$. This suggests that both the glass matrix and Li₆PS₅(BH₄) phase display high lithium-ion conductivities. It is deemed necessary to synthesize single Li₆PS₅(BH₄) phase crystals and examine their conductivity in the future.

All-solid-state cells using mechanochemically prepared Li₂S-P₂S₅-LiBH₄ solid electrolytes with an argyrodite structure were assembled in order to show their potentials for practical applications. Figure 7 shows the charge-discharge curves of the all-solid-state cells using (a) Li/TiS₂, (b) In/LiCoO₂, and (c) In/LiFePO₄ and the $x = 50$ sample. All of the all-solid-state cells using Li₂S-P₂S₅-LiBH₄ was successfully charged and discharged with the large capacities comparable to the previously reported all-solid-state cells.^{2,31} There are few reports of the all-solid-state cells with a LiFePO₄ positive electrode material. The all-solid-state cell using Li metal was also charged and discharged. The Li₂S-P₂S₅-LiBH₄ solid electrolytes have high potential for practical use.

4. CONCLUSIONS

In this study, (100 – x)(0.75Li₂S-0.25P₂S₅)· x LiBH₄ solid electrolytes were prepared by a mechanochemical process. Glassy samples were obtained in the composition range for x (mol %) from 0 to 33, and samples with argyrodite crystalline phase were obtained at $x > 33$. The DSC curves for the samples with LiBH₄ did not exhibit the peak attributed to the phase transition of LiBH₄. The Raman spectra of the (100 – x)(0.75Li₂S-0.25P₂S₅)· x LiBH₄ samples displayed bands attributed to both BH₄⁻ and PS₄³⁻ ions. In the glass-forming region, the conductivity of the glass increased with increasing LiBH₄ content. The $x = 50$ samples that included newly formed crystal phases also exhibited a high conductivity of 1.8×10^{-3} S cm $^{-1}$ at 25 °C and a low conduction activation energy of 16 kJ mol $^{-1}$. Through Rietveld refinements of the $x = 50$ sample, the novel crystal phase was identified as an argyrodite-type crystal, Li₆PS₅(BH₄). The disorder of the S²⁻/BH₄⁻ distribution indicates that the argyrodite-type crystal Li₆PS₅(BH₄) exhibits high lithium-ion conductivity.

AUTHOR INFORMATION

Corresponding Author

*E-mail: hayashi@chem.osakafu-u.ac.jp (A.H.).

ORCID

Atsushi Sakuda: 0000-0002-9214-0347

Akitoshi Hayashi: 0000-0001-9503-5561

Author Contributions

A.S., A.H., and M.T. conceived the study. A.Y., S.Y., and N.K. performed the experiments; A.S., A.Y., S.Y., A.H., and M.T.

wrote the paper. All authors analyzed the data and commented on the manuscript.

Notes

The authors declare no competing financial interest.

REFERENCES

- (1) Hayashi, A.; Sakuda, A.; Tatsumisago, M. Development of Sulfide Solid Electrolytes and Interface Formation Processes for Bulk-Type All-Solid-State Li and Na Batteries. *Front. Energy Res.* **2016**, *4*, 25.
- (2) Kato, Y.; Hori, S.; Saito, T.; Suzuki, K.; Hirayama, M.; Mitsui, A.; Yonemura, M.; Iba, H.; Kanno, R. High-Power All-Solid-State Batteries Using Sulfide Superionic Conductors. *Nat. Energy* **2016**, *1*, 16030.
- (3) Mercier, R.; Malugani, J.-P.; Fahys, B.; Robert, G. Superionic Conduction in Li₂S-P₂S₅-LiI-Glasses. *Solid State Ionics* **1981**, *5*, 663–666.
- (4) Kanno, R.; Murayama, M. Lithium Ionic Conductor Thio-LISICON: The Li₂S-GeS₂-P₂S₅ System. *J. Electrochem. Soc.* **2001**, *148*, A742–A746.
- (5) Hayashi, A.; Hama, S.; Mizuno, F.; Tadanaga, K.; Minami, T.; Tatsumisago, M. Characterization of Li₂S-P₂S₅ Glass-Ceramics as a Solid Electrolyte for Lithium Secondary Batteries. *Solid State Ionics* **2004**, *175*, 683–686.
- (6) Mizuno, F.; Hayashi, A.; Tadanaga, K.; Tatsumisago, M. New, Highly Ion-Conductive Crystals Precipitated from Li₂S-P₂S₅ Glasses. *Adv. Mater.* **2005**, *17*, 918–921.
- (7) Seino, Y.; Ota, T.; Takada, K.; Hayashi, A.; Tatsumisago, M. A Sulphide Lithium Super Ion Conductor Is Superior to Liquid Ion Conductors for Use in Rechargeable Batteries. *Energy Environ. Sci.* **2014**, *7*, 627–631.
- (8) Kamaya, N.; Homma, K.; Yamakawa, Y.; Hirayama, M.; Kanno, R.; Yonemura, M.; Kamiyama, T.; Kato, Y.; Hama, S.; Kawamoto, K.; Mitsui, A. A Lithium Superionic Conductor. *Nat. Mater.* **2011**, *10*, 682–686.
- (9) Sakuda, A.; Hayashi, A.; Tatsumisago, M. Sulfide Solid Electrolyte with Favorable Mechanical Property for All-Solid-State Lithium Battery. *Sci. Rep.* **2013**, *3*, 2261.
- (10) Hayashi, A.; Noi, K.; Sakuda, A.; Tatsumisago, M. Superionic Glass-Ceramic Electrolytes for Room-Temperature Rechargeable Sodium Batteries. *Nat. Commun.* **2012**, *3*, 856.
- (11) Ujiie, S.; Hayashi, A.; Tatsumisago, M. Preparation and Electrochemical Characterization of (100- x)(0.7Li₂S-0.3P₂S₅)- x LiBr Glass-Ceramic Electrolytes. *Mater. Renew. Sustain. Energy* **2014**, *3*, 18.
- (12) Ujiie, S.; Hayashi, A.; Tatsumisago, M. Preparation and Ionic Conductivity of (100- x)(0.8Li₂S-0.2P₂S₅)- x LiI Glass-ceramic Electrolytes. *J. Solid State Electrochem.* **2013**, *17*, 675–680.
- (13) Deiseroth, H.-J.; Kong, S.-T.; Eckert, H.; Vannahme, J.; Reiner, C.; Zaif, T.; Schlosser, M. Li₆PS₅X: A Class of Crystalline Li-Rich Solids with an Unusually High Li $^{+}$ Mobility. *Angew. Chem., Int. Ed.* **2008**, *47*, 755–758.
- (14) Rao, R. P.; Adams, S. Studies of Lithium Argyrodite Solid Electrolytes for All-Solid-State Batteries. *Phys. Status Solidi A* **2011**, *208*, 1804–1807.
- (15) Rayavarapu, P. R.; Sharma, N.; Peterson, V. K.; Adams, S. Variation in Structure and Li $^{+}$ -Ion Migration in Argyrodite-Type Li₆PS₅X (X = Cl, Br, I) Solid Electrolytes. *J. Solid State Electrochem.* **2012**, *16*, 1807–1813.
- (16) Kraft, M. A.; Culver, S. P.; Calderon, M.; Böcher, F.; Krauskopf, T.; Senyshyn, A.; Dietrich, C.; Zevalkink, A.; Janek, J.; Zeier, W. G. Influence of Lattice Polarizability on the Ionic Conductivity in the Lithium Superionic Argyrodites Li₆PS₅X (X = Cl, Br, I). *J. Am. Chem. Soc.* **2017**, *139*, 10909–10918.
- (17) Matsuo, M.; Nakamori, Y.; Orimo, S.-i.; Maekawa, H.; Takamura, H. Lithium Superionic Conduction in Lithium Borohydride Accompanied by Structural Transition. *Appl. Phys. Lett.* **2007**, *91*, 224103.
- (18) Takahashi, K.; Hattori, K.; Yamazaki, T.; Takada, K.; Matsuo, M.; Orimo, S.; Maekawa, H.; Takamura, H. All-Solid-State Lithium

Battery with LiBH₄ Solid Electrolyte. *J. Power Sources* **2013**, *226*, 61–64.

(19) Yamauchi, A.; Sakuda, A.; Hayashi, A.; Kitamura, N.; Idemoto, Y.; Tatsumisago, M. Preparation and Evaluation of Highly Lithium Ion Conductive Li₂S-P₂S₅-LiBH₄ Based Glass-Ceramics. *38th Symposium Solid State Ionics Japan Extension Abstract*, 2012; pp 190–191.

(20) Yamauchi, A.; Sakuda, A.; Hayashi, A.; Tatsumisago, M. Preparation and Ionic Conductivities of (100-x)(0.75Li₂S-0.25P₂S₅)-xLiBH₄ Glass Electrolytes. *J. Power Sources* **2013**, *244*, 707–710.

(21) Unemoto, A.; Wu, H.; Udovic, T. J.; Matsuo, M.; Ikeshoji, T.; Orimo, S.-i. Fast Lithium-Ionic Conduction in a New Complex Hydride–Sulphide Crystalline Phase. *Chem. Commun.* **2016**, *52*, 564–566.

(22) Izumi, F.; Momma, K. Three-Dimensional Visualization in Powder Diffraction. *Solid State Phenom.* **2007**, *130*, 15–20.

(23) Soulié, J.-P.; Renaudin, G.; Černý, R.; Yvon, K. Lithium Boro-Hydride LiBH₄: I. Crystal Structure. *J. Alloys Compd.* **2002**, *346*, 200–205.

(24) Oguchi, H.; Matsuo, M.; Hummelshøj, J. S.; Vegge, T.; Nørskov, J. K.; Sato, T.; Miura, Y.; Takamura, H.; Maekawa, H.; Orimo, S. Experimental and Computational Studies on Structural Transitions in the LiBH₄–LiI Pseudobinary System. *Appl. Phys. Lett.* **2009**, *94*, 141912.

(25) Hayashi, A.; Hama, S.; Minami, T.; Tatsumisago, M. Formation of Superionic Crystals from Mechanically Milled Li₂S–P₂S₅ Glasses. *Electrochem. Commun.* **2003**, *5*, 111–114.

(26) Tachez, M.; Malugani, J.-P.; Mercier, R.; Robert, G. Ionic Conductivity of and Phase Transition in Lithium Thiophosphate Li₃PS₄. *Solid State Ionics* **1984**, *14*, 181–185.

(27) Gomes, S.; Hagemann, H.; Yvon, K. Lithium Boro-Hydride LiBH₄: II. Raman Spectroscopy. *J. Alloys Compd.* **2002**, *346*, 206–210.

(28) Miwa, K.; Ohba, N.; Towata, S.-i.; Nakamori, Y.; Orimo, S.-i. First-Principles Study on Lithium Borohydride LiBH₄. *Phys. Rev. B: Condens. Matter Mater. Phys.* **2004**, *69*, 245120.

(29) Hartman, M. R.; Rush, J. J.; Udovic, T. J.; Bowman, R. C.; Hwang, S.-J. Structure and Vibrational Dynamics of Isotopically Labeled Lithium Borohydride Using Neutron Diffraction and Spectroscopy. *J. Solid State Chem.* **2007**, *180*, 1298–1305.

(30) CRC Handbook of Chemistry and Physics, 88th ed.; Lide, D. R., Ed.; CRC Press, 2007.

(31) Sakuda, A.; Kitaura, H.; Hayashi, A.; Tatsumisago, M.; Hosoda, Y.; Nagakane, T.; Sakamoto, A. All-Solid-State Lithium Secondary Batteries Using Li₂S–P₂S₅ Solid Electrolytes and LiFePO₄ Electrode Particles with Amorphous Surface Layer. *Chem. Lett.* **2012**, *41*, 260–261.